Retrieving the initial-state spin polarization from spin-resolved photoemission: Proposal for a case study on W(110)

Jürgen Henk,[1,*] Koji Miyamoto,[2,3] and Markus Donath[3]

[1]*Institut für Physik, Martin-Luther-Universität Halle-Wittenberg, Von-Seckendorff-Platz 1, 06099 Halle (Saale), Germany*

[2]*Hiroshima Synchrotron Radiation Center, Hiroshima University, 2-313 Kagamiyama, Higashi-Hiroshima 739-0046, Japan*

[3]*Physikalisches Institut, Westfälische Wilhelms-Universität Münster, Wilhelm-Klemm-Strasse 10, 48149 Münster, Germany*

(Received 20 April 2018; revised manuscript received 25 June 2018; published 17 July 2018)

Spin- and angle-resolved photoelectron spectroscopy is commonly used to determine the spin texture of the occupied electronic states. If spin-orbit coupling is strong, the spin polarization of the photoelectrons and that of the initial states may deviate significantly. To alleviate part of this problem we propose a recipe for improved spin retrieval. The basic idea is to combine photoemission intensities from (at least) two different photoemission experiments in a way which reflects the symmetry of the photoemission setups; the procedure avoids group-theoretical analyses or relativistic photoemission calculations. In this paper we introduce the approach, motivated by the example of photoemission from W(110) illuminated by circularly polarized light. Limitations of the method are discussed.

DOI: 10.1103/PhysRevB.98.045124

I. INTRODUCTION

Spin- and angle-resolved photoelectron spectroscopy (SARPES) is considered one of the most used and most versatile experimental techniques to determine the occupied electronic structure of solids in great detail [1–6]. The measured data are commonly interpreted within the one-step or three-step model of photoemission, which allows us—due to conservation of energy E and surface-parallel momentum $\boldsymbol{k}_\parallel$—to determine the energy and wave-vector position of the initial states; the spectral intensities, however, are difficult to interpret because they are essentially determined by the transition matrix elements (dipole interaction). This obstacle is overcome by comparing experimental and theoretical spectra, the latter calculated with sophisticated computer programs in which all major ingredients are taken into account: the electronic structure of the initial and final states with correct boundary conditions, transition matrix elements, light polarization, electron mean free path, etc. [7–10].

If the initial state is intrinsically spin polarized, for example, in a ferromagnet, the above interpretation can be applied to the spin-up and spin-down electrons separately, provided spin-orbit coupling is weak. If, however, spin-orbit coupling is strong, the initial-state spin polarization is not necessarily retrieved in the photoemission experiment. In other words, spin-orbit coupling introduces additional effects to spin-resolved photoemission, which depend on the polarization of the incident light.

Considering circularly polarized light, the photon spin which is aligned parallel or antiparallel with the incidence direction is transferred to the photoelectron [11–13]. In a rough picture, the photoelectron spin becomes more or less aligned with the light incidence direction, that is, "optically oriented." For example, GaAs illuminated by circularly polarized light is a widely used photocathode for spin-polarized electrons.

Linearly polarized light also produces spin-polarized photoelectrons from spin-degenerate initial states [14–19]. However, the spin orientation depends crucially on the light incidence direction and on the geometry of the sample surface.

In a ferromagnet the initial state is intrinsically spin polarized, and the above effects for circularly and linearly polarized light result in magnetic dichroism (that is, the intensity depends on the light polarization) [20–22]; the intensity change is then attributed to the strength of the spin-orbit coupling within the initial state at the chosen $(E, \boldsymbol{k}_\parallel)$ position. The interpretation is facilitated by the fact that the spin texture is collinear.

For noncollinear spin textures of the initial states, prominent examples of which are surface states of Rashba systems (see Refs. [23–26] for selected publications) and of topological insulators (see Refs. [27–37] for selected publications), such an interpretation is difficult without imposing *a priori* assumptions on the spin texture or without help of photoemission calculations.

The above raises a question on how to retrieve the spin polarization of the initial state from a photoemission experiment without referring to assumptions or to relativistic photoemission calculations. This is, of course, not possible in the strict sense since the transition matrix elements govern the intensities. However, one could *combine spectra* taken with different light polarizations or at different $\boldsymbol{k}_\parallel$ in such a way that the spin-orbit effects in the photoemission process are mostly removed. These combinations should, on the one hand, reproduce as faithfully as possible the initial-state spin texture and, on the other hand, provide a measure which tells that the interpretation of these combined spectra has to be done cautiously. Such a combination procedure requires us to take spectra for at least two different setups [38], which in view of the latest developments (e. g., time-of-flight detectors and photoelectron microscopes [39–42]) is not too cumbersome. It

*Corresponding author: juergen.henk@physik.uni-halle.de

also avoids tedious group-theoretical considerations; instead, it relies on a brief symmetry analysis of the photoemission setup.

In this paper we introduce the procedure by considering an admittedly simple but well-understood system: the Dirac-type surface state of W(110). This outstanding surface state has been investigated in great detail; a by no means complete selection of publications includes Refs. [43–50]. We have applied the approach successfully to other paradigmatic systems with spin-polarized surface states, namely, Au(111), Bi/Ag(111), and Bi_2Te_3 (not shown here).

Before introducing our approach, some comments on the purpose of the paper seem appropriate. Our aim is not to consider all possible combinations of light polarization, incidence direction, surface geometries (including, e.g., adlayers), etc. We choose instead a system which lends itself to our study: the Dirac-type surface state on W(110). Since its spin texture and orbital composition are well known, any deviation of the measured photoelectron's spin polarization from that of the surface state can be attributed to the photoemission process. This allows us to introduce and to check our proposal in full clarity.

The dependence of spin-resolved photoemission intensities on various parameters has been determined by theory, with various degree of sophistication (to name a few, Refs. [20,51,52]). A comparison of results obtained from sometimes elaborate formulas with their experimental equivalents allows us to extract the spin polarization that is attributed to the photoemission process. This has convincingly been demonstrated for Gd by Cherepkov and Fecher [8], with emphasis on atomic levels. However, such a comparison could become involved and could require additional input (e.g., from photoemission calculations). In this respect, our purposely simpler approach might be viewed as "self-contained." Although the spin polarization of photoelectrons is governed by a number of effects, the measured intensities contain information on the initial-state spin polarization, which therefore can be extracted by a symmetry-based recipe.

This paper is outlined as follows. In Sec. II we provide the details of the electronic-structure and photoemission calculations as well as the photoemission experiments. Section III introduces the photoemission setups (Sec. III A) and presents spin- and angle-resolved photoemission data for W(110) (Sec. III B); we then proceed with a detailed analysis of these results (Sec. III C). Furthermore, we briefly discuss a chiral setup (Sec. III D). Conclusions are given in Sec. IV. In the Appendix data for linearly polarized light are briefly presented.

II. THEORETICAL AND EXPERIMENTAL ASPECTS

The calculations of the surface electronic structure and of the photoemission intensities follow closely those of Ref. [48]; therefore, we merely repeat the essentials in brief and refer to that publication for details.

The electronic structure of the semi-infinite system has been calculated within the framework of the spin-density approximation to density-functional theory. In a first step, *ab initio* potentials were computed within a full-potential all-electron method [53] and were subsequently transferred to our computer code for relativistic multiple-scattering calculations, the latter relying on so-called muffin-tin potentials. This Korringa-Kohn-Rostoker code solves the Dirac equation; hence, relativistic effects, in particular the spin-orbit interaction, are fully taken into account. The result is the site-resolved spectral density

$$N_i(E+\mathrm{i}\eta, \boldsymbol{k}_\parallel) = -\frac{1}{\pi}\,\mathrm{Im\,Tr}\, G_{ii}(E+\mathrm{i}\eta, \boldsymbol{k}_\parallel), \qquad (1)$$

which is computed from the site-diagonal block G_{ii} of the Green's function of the semi-infinite system (i site index). η accounts for the lifetime broadening and is chosen as in the photoemission calculations. Surface relaxations have been considered as well [54].

The spectral density N_i gives access to the degree of spin polarization for a given spin-quantization axis (SQA) μ, for example, $\mu = x$, y, or z. In the following we show spin differences

$$N_{i;\uparrow\mu}(E+i\eta, \boldsymbol{k}_\parallel) - N_{i;\downarrow\mu}(E+i\eta, \boldsymbol{k}_\parallel), \qquad (2)$$

in which spin up ($\uparrow$) and spin down ($\downarrow$) are defined with respect to the chosen spin-quantization axis μ. We prefer spin differences to spin polarizations because they are small for small intensities, thereby avoiding sizable spin polarizations in regions with small intensities.

Spin-resolved photoemission intensities have been computed within the relativistic one-step model of photoemission, as formulated in multiple-scattering theory [7,10]. Many-particle effects are taken into account by a heuristic self-energy, whose imaginary part leads to broadening of the intensity maxima (lifetime broadening) and to a finite escape depth of the photoelectrons [2]. The result is intensities $I_{\uparrow\mu}$ and $I_{\downarrow\mu}$ that are spin resolved with respect to the chosen spin-quantization axis μ. Spin differences in the photoemission intensities are given as $\Delta_\mu = I_{\uparrow\mu} - I_{\downarrow\mu}$.

For the experimental data, a clean W(110) surface was obtained using the same procedures as described in the literature [44]. The surface quality was confirmed by a sharp (1×1) low-energy electron diffraction pattern with low background intensity, which reflects the C_{2v} symmetry, and by Auger electron spectra. The photoemission experiments were performed at beamline BL-9B of the Hiroshima Synchrotron Radiation Center (HiSOR), which is equipped with highly efficient three-dimensional spin-polarization analysis of the ESPRESSO (Efficient SPin REsolved SpectroScopy Observation) machine [55]. Circularly polarized light of 43 eV energy at an incidence angle of 50° with respect to the electron analyzer was used in our study. Details of the experiment are given elsewhere [56].

III. RESULTS AND DISCUSSION

To illustrate the approach, we address circularly polarized light (with helicities $\sigma_\pm$) that impinges off normally onto the W(110) surface. The photoelectrons are always detected in the $\overline{\Gamma H}$ mirror plane (xz plane; z surface normal), which hosts the strongly spin polarized and linear dispersive Dirac-type surface state.

Details of the Dirac-type surface state have been reported in a considerable number of both theoretical and experimental publications; a comprehensive analysis is given, for example,

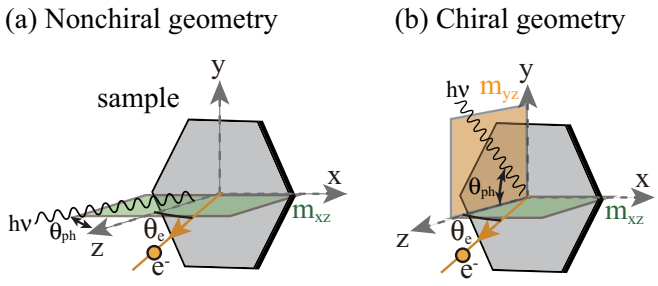

FIG. 1. Photoemission geometries used in the analysis of the proposed recipe. (a) In the nonchiral geometry, light with photon energy $h\nu$ impinges within the xz plane (green) onto the surface (gray); photoelectrons (e^-) are also detected within this plane. (b) In the chiral geometry, the light impinges within the yz plane, while photoelectrons are detected in the xz plane. In both panels, the spin polarization of the initial state is along the y axis. Concerning W(110), the $\overline{\Gamma H}$ ($\overline{\Gamma N}$) azimuth refers to the xz (yz) plane.

in Refs. [47,49]. Thus, its spin texture is well understood: in the $\overline{\Gamma H}$ azimuth the spin-polarization vector is perpendicular to this mirror plane (along $+y$ or $-y$); this feature, dictated by (mirror) symmetry, is fully confirmed by group theory and electronic-structure calculations.

A. Photoemission geometries

We apply the recipe to two "generic" geometries (Fig. 1). In both of them, the electron detection is within the $\overline{\Gamma H}$ mirror plane (xz plane), the initial-state energy is fixed ($E - E_F = -1.1$ eV), and the photon energy is $h\nu = 43$ eV.

In the *nonchiral geometry*, the light impinges also within the $\overline{\Gamma H}$ plane [Fig. 1(a)]; the light incidence direction, surface normal, and electron detection direction are coplanar. The angle between the light incidence and the lens axis of the electron spectrometer is fixed at 50°; hence, intensities for $+k_x$ differ from those for $-k_x$.

In the *chiral geometry* the light impinges within the $\overline{\Gamma N}$ plane (yz plane) onto the surface [Fig. 1(b); the vectors of light incidence direction, surface normal, and electron detection direction span a finite volume, hence the term "chiral"]. Since the $\overline{\Gamma N}$ plane is also a mirror plane of the surface, the relation $I(\sigma_\pm, k_x) = I(\sigma_\mp, -k_x)$ holds, and we expect dichroism, i.e., $I(\sigma_\pm, k_x) \neq I(\sigma_\mp, k_x)$.

B. Photoemission experiments and calculations

To motivate the proposed recipe, we compare experimental and theoretical photoemission spectra for W(110) for the nonchiral geometry. For linearly polarized light, the agreement of experimental and theoretical spectra has been proved in a recent publication [50]. Concerning the circularly polarized light chosen here, we refer to spin-resolved intensity maps of the $\overline{\Gamma H}$ line in Fig. 2 [56].

The Dirac-type surface state (DSS) is clearly identified by its linear dispersion. The spin differences Δ_y for the spin-quantization axis y (middle panels of Fig. 2) reveal its typical spin texture, that is, a sign reversal when turning k_x into $-k_x$. On top of this, this spin texture is robust against helicity reversal: it is, at first sight, unchanged. This finding

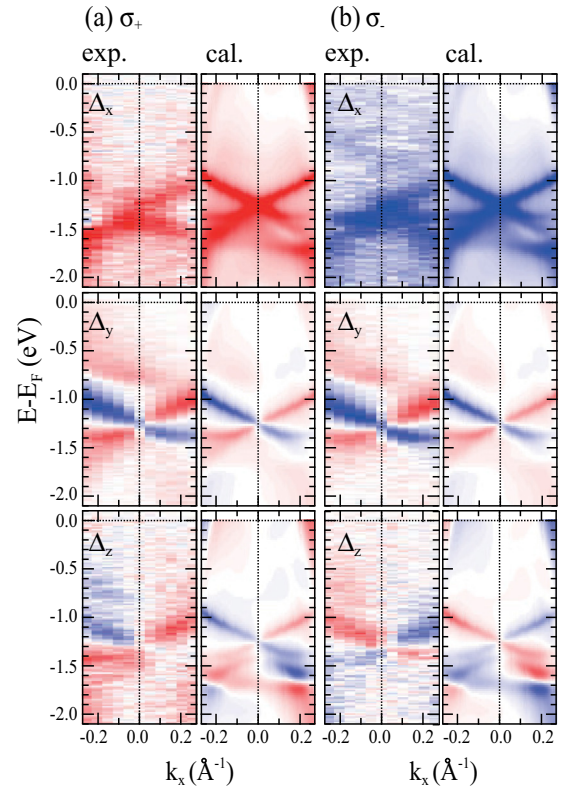

FIG. 2. Experimental and calculated spin-resolved photoemission in the nonchiral geometry from W(110) for the $\overline{\Gamma H}$ azimuth. Spin differences are shown by the color scale (blue: positive; white: zero; red: negative). (a) Spin differences for the spin-quantization axes x, y, and z (from top to bottom) and left-handed circularly polarized light. (b) Spin differences as in (a), but for right-handed circularly polarized light [56].

suggests a strong initial-state spin polarization and a moderate effect of optical orientation.

For the spin-quantization axis z we find a change of sign with k_x *and* with helicity (bottom panels of Fig. 2). This finding points to a mixture of intrinsic spin polarization and optical orientation. Thus, it is hard to conclude on the degree of the initial-state spin polarization without further analysis. As we will see below, this spin difference can be exclusively attributed to optical orientation.

The spin differences for the spin-quantization axis x (top panels of Fig. 2) are symmetric in k_x but change sign upon helicity reversal, which is a clear hint of their origin, namely, optical orientation.

The experimental intensity distributions are reproduced by the theoretical calculations, which puts the following analysis on a firm basis.

C. Analysis of the nonchiral geometry

1. Symmetry analysis

As a first step, we perform a symmetry analysis of the nonchiral photoemission geometry. The light is incident within the xz mirror plane of the semi-infinite system. Upon reflection at the xz plane, the y component of the electric field vector

TABLE I. Symmetry analysis for circularly polarized light incident in the xz plane and photoelectron detection in the xz plane ($k_y = 0$). Here 1, m_{xz}, and m_{yz} denote the trivial and reflection operations, respectively, and C_2 is the rotation by 180° about the z axis. The electric field vector of the incident light reads $\boldsymbol{E} = (E_x, E_y, E_z)$, and that of the photoelectron spin polarization reads $\boldsymbol{P} = (P_x, P_y, P_z)$.

Operation	Light				Photoelectron			
1	E_x	E_y	E_z	$\sigma_\pm$	k_x	P_x	P_y	P_z
m_{xz}	E_x	$-E_y$	E_z	$\sigma_\mp$	k_x	$-P_x$	P_y	$-P_z$
m_{yz}	$-E_x$	E_y	E_z	$\sigma_\mp$	$-k_x$	P_x	$-P_y$	$-P_z$
C_2	$-E_x$	$-E_y$	E_z	$\sigma_\pm$	$-k_x$	$-P_x$	$-P_y$	P_z

$\boldsymbol{E} = (E_x, E_y, E_z)$ changes sign (row m_{xz} in Table I), which also reverses the helicity from right-handed (σ_+) to left-handed (σ_-) or vice versa.

The spin polarization $\boldsymbol{P}$ is a pseudovector, which implies that its coplanar components (P_x and P_z) change sign under the reflection m_{xz} and P_y is conserved. On the one hand, this tells us that the spin polarization of all initial states in the xz mirror plane, in particular of the Dirac-type surface state, is along the y axis (normal to the mirror plane; its degree remains unspecified). On the other hand, the analysis tells us how to combine spectra taken for both helicities to retrieve $\boldsymbol{P}$.

2. Intensity differences

In the following, ↑ and ↓ refer to a chosen spin-quantization axis μ, where $\mu = x$, y, or z. Having chosen a spin-quantization axis μ, one measures the intensities $I_{\uparrow\mu}(\sigma_+)$, $I_{\downarrow\mu}(\sigma_+)$, $I_{\uparrow\mu}(\sigma_-)$, and $I_{\downarrow\mu}(\sigma_-)$ for a specified (E, k_x). This allows us to define the cumulative photocurrent

$$I_0 \equiv I_{\uparrow\mu}(\sigma_+) + I_{\downarrow\mu}(\sigma_+) + I_{\uparrow\mu}(\sigma_-) + I_{\downarrow\mu}(\sigma_-) \qquad (3)$$

and three intensity differences. The latter are easily derived from a decomposition of the intensities into intrinsic and extrinsic parts, $I = I_{\text{int}} + I_{\text{ext}}$. I_{ext} changes sign upon helicity reversal, while I_{int} does not; in other words, I_{ext} stems from optical orientation, and I_{int} stems from the initial-state spin polarization.

(i) In the "intrinsic" intensity difference

$$\Delta_{\text{int}} \equiv I_{\uparrow\mu}(\sigma_+) - I_{\downarrow\mu}(\sigma_+) + I_{\uparrow\mu}(\sigma_-) - I_{\downarrow\mu}(\sigma_-), \qquad (4)$$

which is the sum of the spin differences $\Delta_\mu(\sigma_+) + \Delta_\mu(\sigma_-)$, the effect of the light helicity is averaged out. If the photoemission process itself ("optical orientation") were to produce no spin polarization of the photoelectrons, then the spin-resolved intensities would not depend on the helicity: $I_{\uparrow\mu}(\sigma_+) = I_{\uparrow\mu}(\sigma_-)$ and $I_{\downarrow\mu}(\sigma_+) = I_{\downarrow\mu}(\sigma_-)$. Hence, Δ_{int} captures the intrinsic spin difference, i.e., that of the initial state.

(ii) With the "extrinsic" intensity difference

$$\Delta_{\text{ext}} \equiv I_{\uparrow\mu}(\sigma_+) - I_{\downarrow\mu}(\sigma_+) - I_{\uparrow\mu}(\sigma_-) + I_{\downarrow\mu}(\sigma_-), \qquad (5)$$

which is the difference between the spin differences $\Delta_\mu(\sigma_+) - \Delta_\mu(\sigma_-)$, one detects the effect of the optical orientation. For perfect optical orientation, $I_{\uparrow\mu}(\sigma_+) = I_{\downarrow\mu}(\sigma_-)$ and $I_{\downarrow\mu}(\sigma_+) = I_{\uparrow\mu}(\sigma_-)$. Then Δ_{ext} would be the extrinsic spin difference, i.e., that due to the photoemission process itself.

(iii) The "dichroic" intensity difference

$$\Delta_{\text{dich}} \equiv I_{\uparrow\mu}(\sigma_+) + I_{\downarrow\mu}(\sigma_+) - I_{\uparrow\mu}(\sigma_-) - I_{\downarrow\mu}(\sigma_-) \qquad (6)$$

captures the dichroism, that is, the change of the spin-integrated photocurrents with respect to reversal of the light helicity. In a highly symmetric geometry, Δ_{dich} would vanish. It therefore provides a kind of measure for the quality or for the suitability of the geometry.

3. Application of the recipe

We now apply the analysis to the nonchiral geometry (Fig. 3). The cumulative photocurrent I_0 shows two prominent maxima that stem from the Dirac-type surface state [marked DSS in Fig. 3(a)]; the other maxima at polar angles θ_e of about ±9° are due to emission from a bulk band edge.

For all spin-quantization axes, the dichroic intensity differences vanish, which suggests strongly that this geometry is appropriate for spin retrieval. On top of this, for SQA x [Fig. 3(b)] and SQA z [Fig. 3(d)] there is only a nonzero extrinsic intensity difference, which tells us that the associated photoelectron spin polarizations are exclusively brought about by optical orientation, which is fully in line with the symmetry analysis (Sec. III C 1). Note that Δ_{ext} for the spin-quantization axis x is very strong and almost as large as the intrinsic intensity difference for the spin-quantization axis y.

That the nonchiral geometry "works properly" is established by the fact that only Δ_{int} is nonzero for the spin-quantization axis y, which exhibits the prominent plus-minus feature at the DSS positions. Δ_{int} coincides astonishingly well with the spin difference Δ_y of the initial state [dashed line in Fig. 3(c)]. The latter is obtained from the spin-resolved spectral density (SD) of the outermost W layer. The deviations of the spectral density and the intrinsic photoemission asymmetry are attributed to the transition matrix elements.

Knowing that the initial-state spin polarization P_y changes sign when turning k_x into $-k_x$ (due to time-reversal symmetry; Table I) suggests "postprocessing" or ''antisymmetrizing" Δ_{int}. The result is depicted in Fig. 3(c) as a dashed blue line (labeled int procd) and fits the spectral density very well, in particular in the region of the surface state.

We briefly recapitulate the recipe. (i) Perform a symmetry analysis of the setup. This requires only basic information on the photoemission setup and on the surface geometry. (ii) With the symmetry analysis at hand, define photoemission intensity differences. (iii) Analyze and interpret the intensity differences that have been computed from the measured spin-resolved intensities. (iv) If possible and desired, postprocess the (intrinsic) intensity differences.

4. Limitations of the recipe

From the above one might be tempted to conclude that the recipe is kind of a panacea; that is definitely not the case, as we will show now. The reason for interpreting the results with care is that the transition matrix elements still govern the (spin-resolved) intensities, and the effects of the transition matrix elements cannot be completely removed by taking intensity differences.

The intensities depend on details of the involved electronic states, which change with energy and wave vector. For a

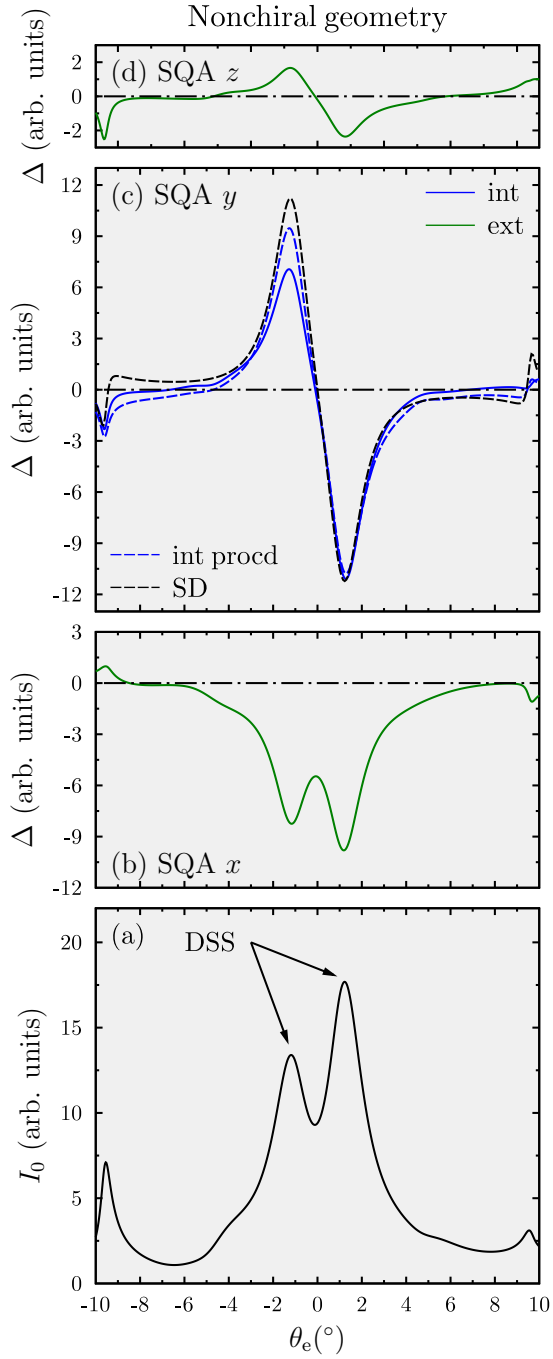

FIG. 3. Theoretical photoemission in the nonchiral geometry. (a) Cumulative intensity I_0, defined in Eq. (3). DSS marks the intensity maxima of the Dirac-type surface state. (b)–(d) Intensity differences Δ_{int} (blue) and Δ_{ext} (green), defined in Eqs. (4) and (5), for the spin quantization axes x [SQA x, panel (b)], y [SQA y, panel (c)], and z [SQA z, panel (d)]; vanishing intensities are not shown. The blue dashed line (int procd) in (c) reproduces the symmetrized intrinsic asymmetry, whereas the black dashed line (SD) is the initial state's spin difference in the topmost W layer scaled roughly to match the black dashed spectrum. θ_e is the polar angle of electron detection. Details of the setup are given in the text. The dichroic intensity differences are zero for this geometry.

constant-energy cut, a variation of the photon energy is equivalent to a change in the final state (outgoing photoelectron).

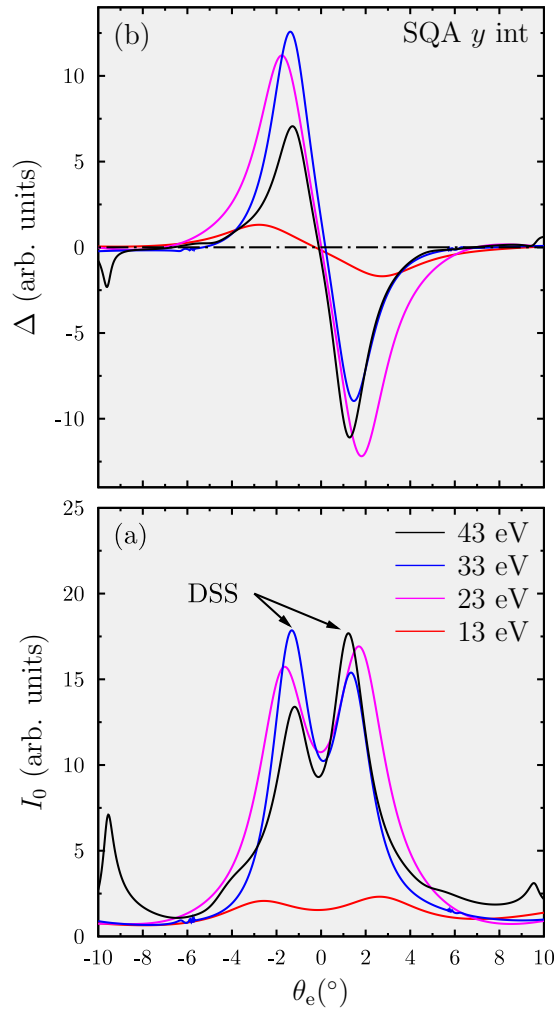

FIG. 4. Theoretical photoemission in the nonchiral geometry for selected photon energies. (a) Cumulative intensities I_0 for photon energies from 13 to 43 eV (as indicated by color). (b) Intrinsic intensity differences Δ_{int} for the spin-quantization axis y. Intensities share a common scale.

For moderate photon energies [23, 33, and 43 eV in Fig. 4(a)] emission from the Dirac-type surface state is strong, in contrast to that for 13 eV (red in Fig. 4), for which the surface state shows up as broad maxima. This weak intensity manifests itself in the associated intrinsic intensity difference, which is comparably weak [Fig. 4(b)]. Nevertheless, the prominent plus-minus feature of the intrinsic spin polarization is clearly resolved.

A second caveat is due to orbital-selective dipole transitions. The Dirac-type surface state is, for the most part, composed of d_{z^2} orbitals (which are aligned along the surface normal). As a result, emission for circularly polarized light is weak if the electric field $\boldsymbol{E}$ shows no sizable z component. This can be understood in an admittedly rather crude picture by assuming a single plane wave as the final state (photoelectron). A transition matrix element can then be written as $(\boldsymbol{E}\cdot\boldsymbol{k})\,\psi_{z^2}(\boldsymbol{k})$, that is, the scalar product of electric field $\boldsymbol{E}$ and photoelectron wave vector $\boldsymbol{k}$ times the Fourier-transformed d_{z^2} orbital. For $\boldsymbol{k}$ close to the surface normal (z axis), the d_{z^2} orbital yields no significant contribution to the photocurrent for (almost) normal incidence

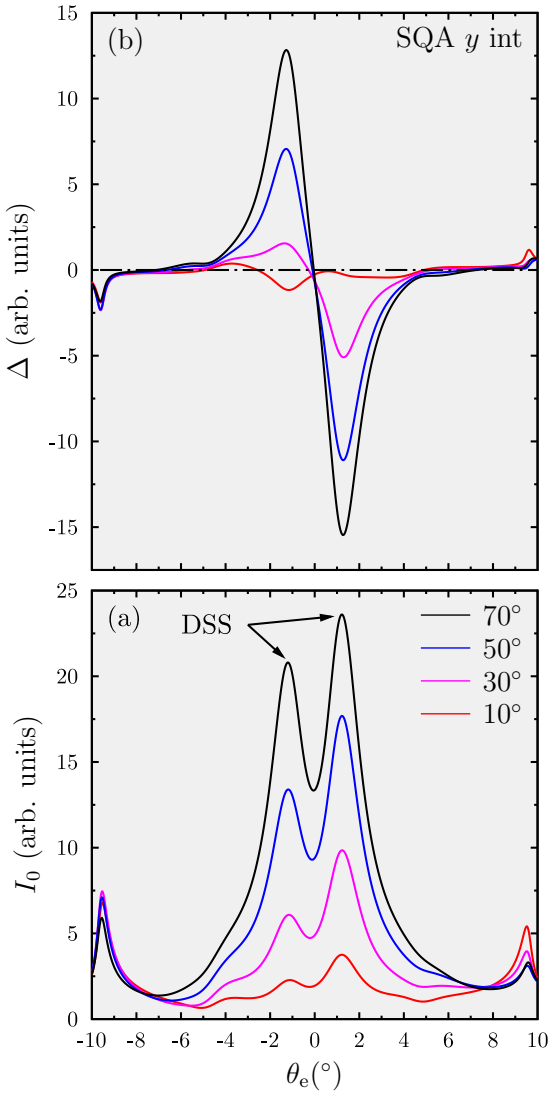

FIG. 5. Theoretical photoemission in the nonchiral geometry for 43 eV photon energy but selected polar angles θ_{ph} of incidence. (a) Cumulative intensities I_0 for θ_{ph} from 10° to 70° (as indicated by color). (b) Intrinsic intensity differences Δ_{int} for the spin-quantization axis y. Intensities share a common scale.

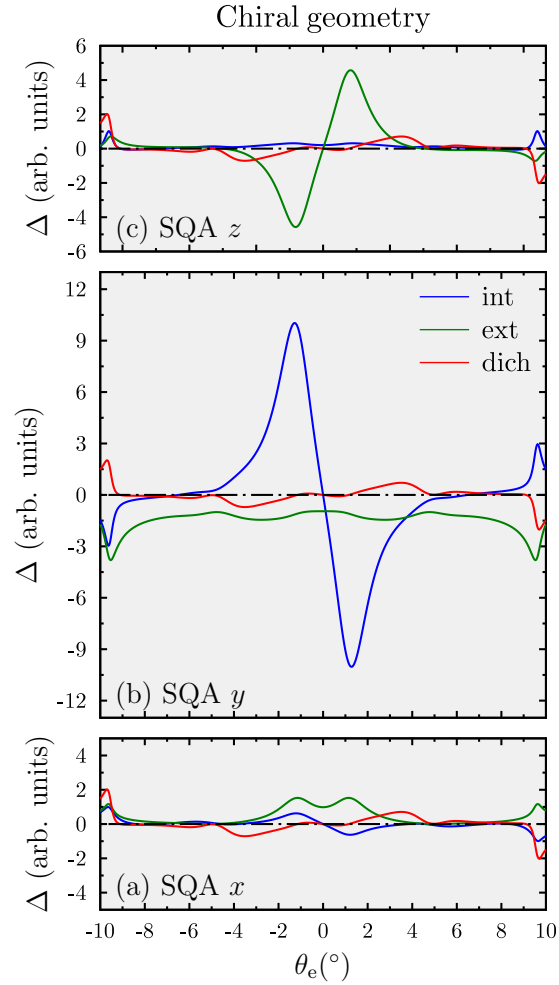

FIG. 6. Theoretical photoemission from the chiral geometry. Intensity differences are as indicated in (b) (see also Fig. 3).

of the light. Therefore, we expect that for polar angles of incidence θ_{ph} close to 0° the surface state's intensity is weak, and like before, the recipe does not work well.

This consideration is nicely confirmed by intensities for a fixed photon energy of 43 eV but varied θ_{ph} (Fig. 5). The larger θ_{ph} lead to strong intensities [Fig. 5(a)] and pronounced plus-minus features in the intrinsic intensity difference [Fig. 5(b)]. The exception is $\theta_{ph} = 10^\circ$: here the in-plane orbitals of the Dirac-type surface state determine both intensity and intrinsic intensity difference (red); the plus-minus feature does not come out.

These findings suggest that the recipe works best when the initial state under consideration shows strong intensities. In each and every case, the results have to be interpreted carefully. We note in passing that the decomposition into intrinsic, extrinsic, and dichroic intensity differences works perfectly in all cases discussed in this section.

D. Analysis of the chiral geometry

It is worth addressing the suitability of the chiral geometry for spin retrieval. The intensity differences are obtained from spectra for circularly polarized light incident within the $+yz$ and $-yz$ azimuths; these setups are related by m_{xz} (Table I). Alternatively, one could use spectra for light incidence within the $+yz$ azimuth but with reversed k_x (setups related by m_{yz}).

The intrinsic intensity differences Δ_{int} are nonzero for all three spin-quantization axes (SQA; Fig. 6). This finding suggests that the Dirac-type surface state should possess nonzero P_x and P_z, which contradicts the symmetry analysis (Sec. III C 1; only P_y should be nonzero). The intrinsic intensity difference for SQA y [Fig. 6(b)] shows a dominating plus-minus feature at the positions of the DSS which complies with the spin texture of this surface state (a change in sign upon reversing θ or k_x; Table I). However, the intensity differences contain signatures that render this geometry inferior for extracting the initial-state spin texture: there are nonzero extrinsic and dichroic intensity differences for all spin-quantization axes.

Recall that P_y of the surface state is very large, which is reflected in the pronounced intrinsic intensity difference for the spin-quantization axis y. Thus, one might be tempted to conclude that the chiral setup is suitable. However, one

should be aware that, usually, the degree of spin polarization is *a priori* unknown if only experimental intensities are available.

IV. CONCLUDING REMARKS

With a focus on systems with strong spin-orbit coupling, we proposed a recipe which puts the retrieval of the spin polarization of initial states from spin- and angle-resolved photoemission data on a more solid basis. The basic idea is to derive intensity differences from a symmetry analysis of the photoemission setup. The intensity differences are computed from photoemission intensities from different photoemission experiments, for example, for two different light helicities. This procedure improves the spin retrieval, and it avoids tedious group-theoretical analyses or demanding relativistic photoemission calculations.

The manipulation of the spin polarization by photoemission has been investigated for Rashba systems and topological insulators (e.g., Ref. [57]). In these publications, the measured spin polarization is often compared to that obtained by electronic-structure calculations. The approach suggested in this paper does not require the calculations; relying solely on the measured intensities, the extrinsic and intrinsic contributions are estimated on equal footing.

An essential question remains: Why are the experimental data (Fig. 2) used to motivate but not to test the recipe? The proposed analysis hinges on accurate determination of photoemission intensity *differences*, which requires that the intensities obtained for both circular polarizations are comparable in absolute value. This condition can be fulfilled if either the photon flux is constant and the surface conditions of the sample are stable or the circular polarization of the light is switched on a rather fast timescale for each data point. Since in our experiment the photon flux decreased with time and the spectra for right- and left-circularly polarized light were taken successively, intensity differences cannot be reliably deduced. Nevertheless, spin-resolved photoelectron spectroscopy with circularly polarized light at third-generation synchrotrons with stable photon flux and fast switching of the circular polarization promise successful use of the proposed recipe: the experimental retrieval of the initial-state spin polarization from spin- and angle-resolved photoelectron spectroscopy without the help of photoemission calculations.

APPENDIX: NONCHIRAL GEOMETRY AND *p*-POLARIZED LIGHT

We briefly address the nonchiral geometry for p-polarized light. Since the angle between electron detection and light incidence is fixed (50°), the intensity is asymmetric, $I(k_x) \neq I(-k_x)$. This suggests combining intensities for k_x and $-k_x$ to define the intensity differences,

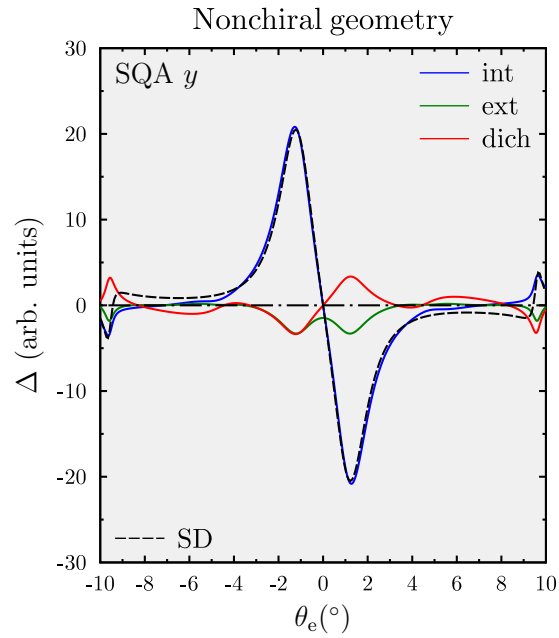

FIG. 7. Theoretical photoemission from the nonchiral geometry but with p-polarized light. Intensity differences are as indicated. Only data for the spin-quantization axis (SQA) y are shown.

$$\Delta_{\text{int}} \equiv I_{\uparrow\mu}(+k_x) - I_{\downarrow\mu}(+k_x) - I_{\uparrow\mu}(-k_x) + I_{\downarrow\mu}(-k_x), \tag{A1}$$

$$\Delta_{\text{ext}} \equiv I_{\uparrow\mu}(+k_x) - I_{\downarrow\mu}(+k_x) + I_{\uparrow\mu}(-k_x) - I_{\downarrow\mu}(-k_x), \tag{A2}$$

$$\Delta_{\text{dich}} \equiv I_{\uparrow\mu}(+k_x) + I_{\downarrow\mu}(+k_x) - I_{\uparrow\mu}(-k_x) - I_{\downarrow\mu}(-k_x). \tag{A3}$$

Δ_{dich} reflects the mentioned k_x asymmetry of the intensity.

For all three spin-quantization axes, the dichroic intensity differences are nonzero, are antisymmetric in k_x, and exhibit identical shape (red line in Fig. 7; only data for SQA y are shown). The other intensity differences are zero for spin-quantization axes x and z.

In addition to its dichroic part, the spin difference along y is composed of two contributions: the extrinsic contribution (green line) is due to the photoemission effect predicted in Ref. [15]; it is symmetric in k_x. The intrinsic one is due to the Dirac-type surface state (blue line) and fits nicely the spin difference obtained from the spectral density (dashed line). Thus, we conclude that the proposed approach works reasonably well but is inferior to the nonchiral geometry with circularly polarized light.

[1] J. Kirschner, *Polarized Electrons at Surfaces* (Springer, London, 1985).

[2] *Polarized Electrons in Surface Physics*, edited by R. Feder, Advanced Series in Surface Science (World Scientific, Singapore, 1985).

[3] J. Kessler, *Polarized Electrons*, 2nd ed., Springer Series on Atoms and Plasmas Vol. 1 (Springer, Berlin, 1985).

[4] *Solid-State Photoemission and Related Methods: Theory and Experiment*, edited by W. Schattke and M. A. van Hove (Wiley-VCH, Weinheim, 2003).

[5] J. Osterwalder, in *Magnetism: A Synchrotron Radiation Approach*, Lecture Notes in Physics Vol. 697 (Springer, Berlin, 2006), p. 95.

[6] U. Heinzmann and J. H. Dil, J. Phys.: Condens. Matter **24**, 173001 (2012).

[7] J. Braun, Rep. Prog. Phys. **59**, 1267 (1996).

[8] N. A. Cherepkov and G. H. Fecher, Phys. Rev. B **61**, 2561 (2000).

[9] J. Braun and M. Donath, J. Phys.: Condens. Matter **16**, S2539 (2004).

[10] J. Henk, in *Handbook of Thin Film Materials*, edited by H. S. Nalwa (Academic, San Diego, 2002), Vol. 2, Chap. 10, p. 479.

[11] U. Fano, Phys. Rev. **178**, 131 (1969).

[12] U. Fano, Phys. Rev. **184**, 250 (1969).

[13] J. Minár, H. Ebert, G. Ghiringhelli, O. Tjernberg, N. B. Brookes, and L. H. Tjeng, Phys. Rev. B **63**, 144421 (2001).

[14] E. Tamura, W. Piepke, and R. Feder, Phys. Rev. Lett. **59**, 934 (1987).

[15] E. Tamura and R. Feder, Europhys. Lett. **16**, 695 (1991).

[16] J. Henk and R. Feder, Europhys. Lett. **28**, 609 (1994).

[17] B. Schmiedeskamp, N. Irmer, R. David, and U. Heinzmann, Appl. Phys. A **53**, 418 (1991).

[18] N. Irmer, R. David, B. Schmiedeskamp, and U. Heinzmann, Phys. Rev. B **45**, 3849 (1992).

[19] N. Irmer, F. Frentzen, S.-W. Yu, B. Schmiedeskamp, and U. Heinzmann, J. Electron Spectrosc. Relat. Phenom. **78**, 321 (1996).

[20] J. Henk, T. Scheunemann, S. V. Halilov, and R. Feder, J. Phys.: Condens. Matter **8**, 47 (1996).

[21] H. Ebert, J. Minár, and V. Popescu, in *Band-Ferromagnetism: Ground-State and Finite-Temperature Phenomena*, edited by K. Baberschke, W. Nolting, and M. Donath, Lecture Notes in Physics Vol. 580 (Springer, Berlin, 2001), p. 371.

[22] W. Kuch and C. M. Schneider, Rep. Prog. Phys. **64**, 147 (2001).

[23] M. Hoesch, M. Muntwiler, V. N. Petrov, M. Hengsberger, L. Patthey, M. Shi, M. Falub, T. Greber, and J. Osterwalder, Phys. Rev. B **69**, 241401(R) (2004).

[24] J. Henk, M. Hoesch, J. Osterwalder, A. Ernst, and P. Bruno, J. Phys.: Condens. Matter **16**, 7581 (2004).

[25] C. R. Ast, J. Henk, A. Ernst, L. Moreschini, M. C. Falub, D. Pacilé, P. Bruno, K. Kern, and M. Grioni, Phys. Rev. Lett. **98**, 186807 (2007).

[26] G. Bihlmayer, S. Blügel, and E. V. Chulkov, Phys. Rev. B **75**, 195414 (2007).

[27] H. Zhang, C.-X. Liu, X.-L. Qi, Z. Fang, and S.-C. Zhang, Nat. Phys. **5**, 438 (2009).

[28] D. Hsieh, Y. Xia, L. Wray, D. Quian, A. Pal, J. H. Dil, J. Osterwalder, F. Meier, G. Bihlmayer, C. L. Kane *et al.*, Science **323**, 919 (2009).

[29] D. Hsieh, Y. Xia, D. Qian, L. Wray, F. Meier, J. H. Dil, J. Osterwalder, L. Patthey, A. V. Fedorov, H. Lin *et al.*, Phys. Rev. Lett. **103**, 146401 (2009).

[30] S. Souma, K. Kosaka, T. Sato, M. Komatsu, A. Takayama, T. Takahashi, M. Kriener, K. Segawa, and Y. Ando, Phys. Rev. Lett. **106**, 216803 (2011).

[31] W. Jung, Y. Kim, B. Kim, Y. Koh, C. Kim, M. Matsunami, S.-I. Kimura, M. Arita, K. Shimada, J. H. Han *et al.*, Phys. Rev. B **84**, 245435 (2011).

[32] C. Jozwiak, Y. L. Chen, A. V. Fedorov, J. G. Analytis, C. R. Rotundu, A. K. Schmid, J. D. Denlinger, Y.-D. Chuang, D.-H. Lee, I. R. Fisher *et al.*, Phys. Rev. B **84**, 165113 (2011).

[33] S. Basak, H. Lin, L. A. Wray, S.-Y. Xu, L. Fu, M. Z. Hasan, and A. Bansil, Phys. Rev. B **84**, 121401 (2011).

[34] T. Valla, Z.-H. Pan, D. Gardner, Y. S. Lee, and S. Chu, Phys. Rev. Lett. **108**, 117601 (2012).

[35] J. W. McIver, D. Hsieh, H. Steinberg, P. Jarillo-Herrero, and N. Gedik, Nat. Nanotechnol. **7**, 96 (2012).

[36] S. R. Park, J. Han, C. Kim, Y. Y. Koh, C. Kim, H. Lee, H. J. Choi, J. H. Han, K. D. Lee, N. J. Hur *et al.*, Phys. Rev. Lett. **108**, 046805 (2012).

[37] H. Mirhosseini and J. Henk, Phys. Rev. Lett. **109**, 036803 (2012).

[38] By *geometry* we refer to the light incidence direction, electron detection direction, and surface structure. By *setup* we mean the geometry *and* the chosen light polarization. The setups are related by a symmetry operation. The proposed approach relies on a comparison of intensities for at least two setups with identical geometry, for example, left- and right-handed circularly polarized light in the nonchiral geometry.

[39] G. Schönhense, A. Oelsner, O. Schmidt, G. H. Fecher, V. Mergel, O. Jagutzki, and H. Schmidt-Böcking, Surf. Sci. **480**, 180 (2001).

[40] A. Oelsner, M. Rohmer, C. Schneider, D. Bayer, G. Schönhense, and M. Aeschlimann, J. Electron Spectrosc. Relat. Phenom. **178–179**, 317 (2010).

[41] C. Tusche, A. Krasyuk, and J. Kirschner, Ultramicroscopy **159**, 520 (2015).

[42] K. Medjanik, O. Fedchenko, S. Chernov, D. Kutnyakhov, M. Ellguth, A. Oelsner, B. Schönhense, T. R. F. Peixoto, P. Lutz, C.-H. Min, F. Reinert, S. Däster, Y. Acremann, J. Viefhaus, W. Wurth, H. J. Elmers, and G. Schönhense, Nat. Mater. **16**, 615 (2017).

[43] R. H. Gaylord and S. D. Kevan, Phys. Rev. B **36**, 9337 (1987).

[44] K. Miyamoto, A. Kimura, K. Kuroda, T. Okuda, K. Shimada, H. Namatame, M. Taniguchi, and M. Donath, Phys. Rev. Lett. **108**, 066808 (2012).

[45] K. Miyamoto, A. Kimura, T. Okuda, K. Shimada, H. Iwasawa, H. Hayashi, H. Namatame, M. Taniguchi, and M. Donath, Phys. Rev. B **86**, 161411(R) (2012).

[46] A. G. Rybkin, E. E. Krasovskii, D. Marchenko, E. V. Chulkov, A. Varykhalov, O. Rader, and A. M. Shikin, Phys. Rev. B **86**, 035117 (2012).

[47] H. Mirhosseini, M. Flieger, and J. Henk, New J. Phys. **15**, 033019 (2013).

[48] H. Mirhosseini, F. Giebels, H. Gollisch, J. Henk, and R. Feder, New J. Phys. **15**, 095017 (2013).

[49] J. Braun, K. Miyamoto, A. Kimura, T. Okuda, M. Donath, H. Ebert, and J. Minár, New J. Phys. **16**, 015005 (2014).

[50] K. Miyamoto, H. Wortelen, H. Mirhosseini, T. Okuda, A. Kimura, H. Iwasawa, K. Shimada, J. Henk, and M. Donath, Phys. Rev. B **93**, 161403(R) (2016).

[51] S. M. Goldberg, C. S. Fadley, and S. Kono, J. Electron Spectrosc. Relat. Phenom. **21**, 285 (1981).

[52] J. Henk, A. M. N. Niklasson, and B. Johansson, Phys. Rev. B **59**, 13986 (1999).

[53] Forschungszentrum Jülich, The Jülich FLAPW code family: FLEUR, Jülich, Germany, http://www.flapw.de.

[54] D. Thonig, T. Rauch, H. Mirhosseini, J. Henk, I. Mertig, H. Wortelen, B. Engelkamp, A. B. Schmidt, and M. Donath, Phys. Rev. B **94**, 155132 (2016).

[55] T. Okuda, K. Miyamaoto, H. Miyahara, K. Kuroda, A. Kimura, H. Namatame, and M. Taniguchi, Rev. Sci. Instrum. **82**, 103302 (2011).

[56] K. Miyamoto, H. Wortelen, T. Okuda, J. Henk, and M. Donath, Sci. Rep. **8**, 10440 (2018).

[57] C. Jozwiak, C.-H. Park, K. Gotlieb, C. Hwang, D.-H. Lee, S. G. Louie, J. D. Denlinger, C. R. Rotundu, R. J. Birgeneau, Z. Hussain *et al.*, Nat. Phys. **9**, 293 (2013).